remote sensing

MDPI

Article

Thermal Profile Dynamics of a Central European River Based on Landsat Images: Natural and Anthropogenic Influencing Factors

Ahmed Mohsen [1,2], Tímea Kiss [3], Sándor Baranya [4], Alexia Balla [1] and Ferenc Kovács [1,*]

[1] Department of Geoinformatics, Physical and Environmental Geography, University of Szeged, Egyetem Str. 2–6, 6722 Szeged, Hungary; ahmed_mohsen250@f-eng.tanta.edu.eg (A.M.); csumpsz@gmail.com (A.B.)
[2] Department of Irrigation and Hydraulics Engineering, Tanta University, Tanta 31512, Egypt
[3] Independent Researcher, Horváth Gy. Str. 80, 6630 Mindszent, Hungary; kisstimi@gmail.com
[4] Department of Hydraulic and Water Resources Engineering, Budapest University of Technology and Economics, Műegyetem Rkp. 3, 1111 Budapest, Hungary; baranya.sandor@emk.bme.hu
* Correspondence: kovacsf@geo.u-szeged.hu

Abstract: River temperature is a critical parameter influencing aquatic ecosystems and water quality. However, it can be changed by natural (e.g., flow and depth conditions) and human factors (e.g., waste and industrial water drainage). Satellite-based monitoring offers a valuable tool for assessing river temperature on a large scale, elucidating the impacts of various factors. This study aims to analyze the spatiotemporal dynamics of surface water temperature (SWT) in the medium-sized Tisza River in response to natural and anthropogenic influences, employing Landsat satellites and in situ water temperature data. The validity of the Landsat-based SWT estimates was assessed across different channel sections with varying sizes. The longitudinal thermal profile of the Tisza was analyzed by mosaicking, monthly, four Landsat 9 images, covering the entire 962 km length of the Tisza in 2023. The impact of climate change was evaluated by analyzing SWT trends at a specific site from 1984 to 2024, utilizing 483 Landsat 4–9 images. The findings indicated elevated accuracy for Landsat-based SWT estimation ($R^2 = 0.94$; RMSE = 3.66 °C), particularly for channel sizes covering ≥ 3 pixels. Discharge, microclimatic conditions, and channel morphology significantly influence SWT, demonstrating a general increasing trend downstream with occasional decreases during the summer months. Dams were observed to lower the SWT downstream due to cooler bottom reservoir water discharge, with more pronounced differences during the summer months (1–3 °C). Tributaries predominantly (75%) elevated the SWT in the Tisza River, albeit with varying magnitudes across different months. Over the 40-year study period, an increasing trend in SWT was discerned, with an annual rise rate of 0.0684 °C. While the thermal band of Landsat satellites proved valuable for investigating the Tisza River's thermal profile at a broad scale, finer spatial resolution bands are necessary for detecting small-scale phenomena such as thermal plumes and localized temperature variations in rivers.

Keywords: thermal bands; Google Earth Engine (GEE); dams; tributaries; urban heat island; riverbanks

Citation: Mohsen, A.; Kiss, T.; Baranya, S.; Balla, A.; Kovács, F. Thermal Profile Dynamics of a Central European River Based on Landsat Images: Natural and Anthropogenic Influencing Factors. *Remote Sens.* **2024**, *16*, 3196. https://doi.org/10.3390/rs16173196

Academic Editor: Janet Nichol

Received: 2 July 2024
Revised: 21 August 2024
Accepted: 27 August 2024
Published: 29 August 2024

1. Introduction

The surface water temperature (SWT) of rivers is one of the key factors influencing the physical, chemical, and biological characteristics of water and consequently its quality conditions [1]. It has a significant impact on aquatic ecosystem health by controlling the solubility of gases (e.g., dissolved oxygen), chemical reactions, and nutrient cycle rates [2]. The spatiotemporal distribution of temperature in rivers is quite complex, influenced by

several interfering natural (e.g., solar radiation, flow conditions, groundwater inflow, and riparian vegetation) and anthropogenic factors (e.g., thermal pollution, deforestation, construction of dams and reservoirs, urbanization, and climate change). Although several scholars have attempted to investigate these distribution dynamics, they tend to focus on a single factor (e.g., dams and reservoirs [2,3] or groundwater input [4]) or have limited spatiotemporal scales [5]. Hence, further research accounting for the interference effects of these factors at the entire river scale is warranted for comprehensive riverine ecosystem management and mitigation of the impacts of anthropogenic activities.

Investigating longitudinal thermal profiles in rivers is essential for effective river conservation and management efforts. It supports the assessment of anthrophonic activities on the river's temperature, evaluation of the river's thermal regime and adaptability of aquatic organisms, and identification of the locations and persistence of thermal refugia [6]. While several studies have reported a downstream trend in rivers' longitudinal thermal profile e.g., in the Pend Oreille River, USA [6], and the Qingjiang River, China [3], alternative and complex patterns, e.g., uniform, linear, and parabolic forms, have also been documented [7]. This indicates the variability of influencing factors affecting a river's thermal profile (e.g., climate, river size, land use/land cover, groundwater inflow, and anthropogenic activities) as well as their variability from one river to another. Additionally, there has been little evaluation of the persistence of identified longitudinal patterns throughout the year.

Climate change has a significant influence on rivers' thermal profiles, typically increasing their temperature, altering the catchment area of precipitation patterns, the ice melt timing, and the hydrological cycle, as well as exacerbating drought periods [8,9]. Similarly, these changes influence water quality, aquatic ecosystems, and hydrological processes, shedding light on the importance of evaluating the impacts of climate change on rivers, aiming toward more effective measures and mitigation scenarios.

Tributaries play a prominent role in shaping the river's thermal profile. Specifically, they have the potential to discontinue the longitudinal profile [6], forming local cooling or warming zones and causing thermal stratification in the mainstream due to temperature gradients. However, the magnitude of their influence depends mainly on their size, confluence angle, and relative temperature compared to the mainstream. On the other hand, the cumulative impact of multiple tributaries along rivers and their persistent influence throughout the year are still understudied.

While shade provided by riparian vegetation along rivers' floodplains prevents excessive heating of water by reducing direct exposure to solar radiation, groundwater inflow may either cool or warm the river's water based on its relative temperature [10,11]. However, both factors contribute to spatiotemporal variability in the longitudinal thermal profile, leading to the formation of local thermal heterogeneous zones (e.g., cold water refugia) and thermal stratification [11].

Dams appear as one of the most significant anthropogenic factors disrupting the longitudinal thermal profile of rivers and altering their annual thermal cycle [12]. Several studies have reported a decline in the water temperature of rivers downstream of dams owing to the release of cold water from the bottom of the reservoir [3,13]. However, in small dams with shallow reservoirs, an opposite pattern can occur due to the release of warm water from the surface [13]. Furthermore, dams can delay the annual cycle of not only water discharge but also the thermal regime, affecting the timing of maximum and minimum temperatures [12] and the development of ice cover [14].

Industrial activities, especially those involving power plants, the steel industry, and chemical manufacturing as well as wastewater treatment plant (WWTP) effluents, particularly those applying biological treatment technology, may significantly impact rivers' thermal profiles. This can lead to the formation of thermal plumes, thermal stratification, and alterations in river flow, and structure, as well as influencing ecological and chemical processes [15]. However, regulatory and mitigation measures (e.g., cooling technologies and effluent temperature limits) may help alleviate their negative influence. Remarkably,

their influence may change seasonally depending on their relative temperature compared to the river's water [16].

A comprehensive assessment of rivers' thermal profiles necessitates intensive spatiotemporal measurements of water temperature, which is typically labor intensive, costly, and time consuming. In the meantime, thermal infrared (TIR) remote sensing provides a more effective alternative, allowing synoptic monitoring of long river reaches, frequent imaging, and accessibility to inaccessible sections [17]. This technique relies on recording the emitted TIR radiation with a sensor (3–14 μm), providing information about surface water temperature in the "skin" layer (100 μm) [18]. This can be achieved using airborne [19,20] or satellite thermal imaging (e.g., Moderate Resolution Imaging Spectroradiometer (MODIS) [21] and Landsat ETM+ [3]). While space-born TIR imaging provides cost-effective and large-scale coverage, it has a pixel size typically lower than airborne imaging, making it unsuitable for resolving small river channels [18].

Although several studies have investigated the thermal profile of rivers worldwide, a comprehensive assessment of the cumulative influence of various natural and anthropogenic factors at the entire river scale is still understudied. Additionally, the consistent influence of these variables along the river and their persistence throughout the year have yet to be revealed. Moreover, the suitability of medium spatial resolution satellite images in assessing the fine-scale thermal heterogeneity induced by industrial and WWTP effluents is still inadequately studied. Therefore, the main aim of this study is to employ Landsat satellite images to investigate the spatiotemporal distribution and dynamics of rivers' thermal profile throughout the year, considering the lowland, medium-sized Tisza River in Central Europe as a case study. The main goals of the study are to (1) reveal the monthly thermal longitudinal trend of the river and the variability of SWT along river sections, (2) study the influence of dams and tributaries on Tisza's thermal profile, and (3) study the influence of climate change on Tisza's temperature by analyzing the SWT of historical Landsat images (1984–2024) at a particular site in the river, and finally, (4) evaluate the potential of Landsat images for detecting the influence of WWTP effluents on medium-sized rivers.

The novelty of this research lies in applying well-established remote sensing techniques to provide a comprehensive assessment of various natural and anthropogenic factors on SWT dynamics in the Tisza River, considering their cumulative and interacting effects. Unlike previous studies, which usually focus on limited sections of rivers and single influencing factors, this study examined the entire length of the river (962 km), considering the influence of tributaries, dams, groundwater input, urban areas, vegetation cover, shading, and global warming. Additionally, previous studies have typically focused on large rivers, whereas this study highlights the applicability of Landsat-based SWT estimation in medium-sized rivers, evaluating the influence of channel size, hydrology, and geomorphology on SWT estimation accuracy. While advancing remote sensing techniques was not the primary aim of our research, we effectively combined multiple methods (e.g., mosaicking, NDWI, OTSU thresholding, cloud masking, and Mann–Kendall analysis) and utilized the entire Landsat dataset to accomplish the study's main goals. We believe that the application of these well-established techniques in such a detailed and long-term study provides profound value to the scientific community, even if it does not offer new methods.

2. Materials and Methods

2.1. Study Area

The thermal profile of the entire length (962 km) of the medium-sized Tisza River was investigated in detail, employing Landsat TIR images. The Tisza River is the longest tributary of the Danube and its discharge (mean: 930 m^3/s) forms 13% of the Danube's discharge [22]. The Tisza's channel size varies significantly along its course and seasonally (mean width: 150 m [23]). It drains the eastern Carpathian basin (catchment area: 157,000

km²), specifically the mountains and hilly sub-catchments in Ukraine, Slovakia, and Romania, as well as the lowlands in Hungary and Serbia (Figure 1) [24]. The mountainous sub-catchments in the northern and northeastern parts are covered by forests; meanwhile, the lowlands and alluvial plains are characterized by intensive agricultural activities [25].

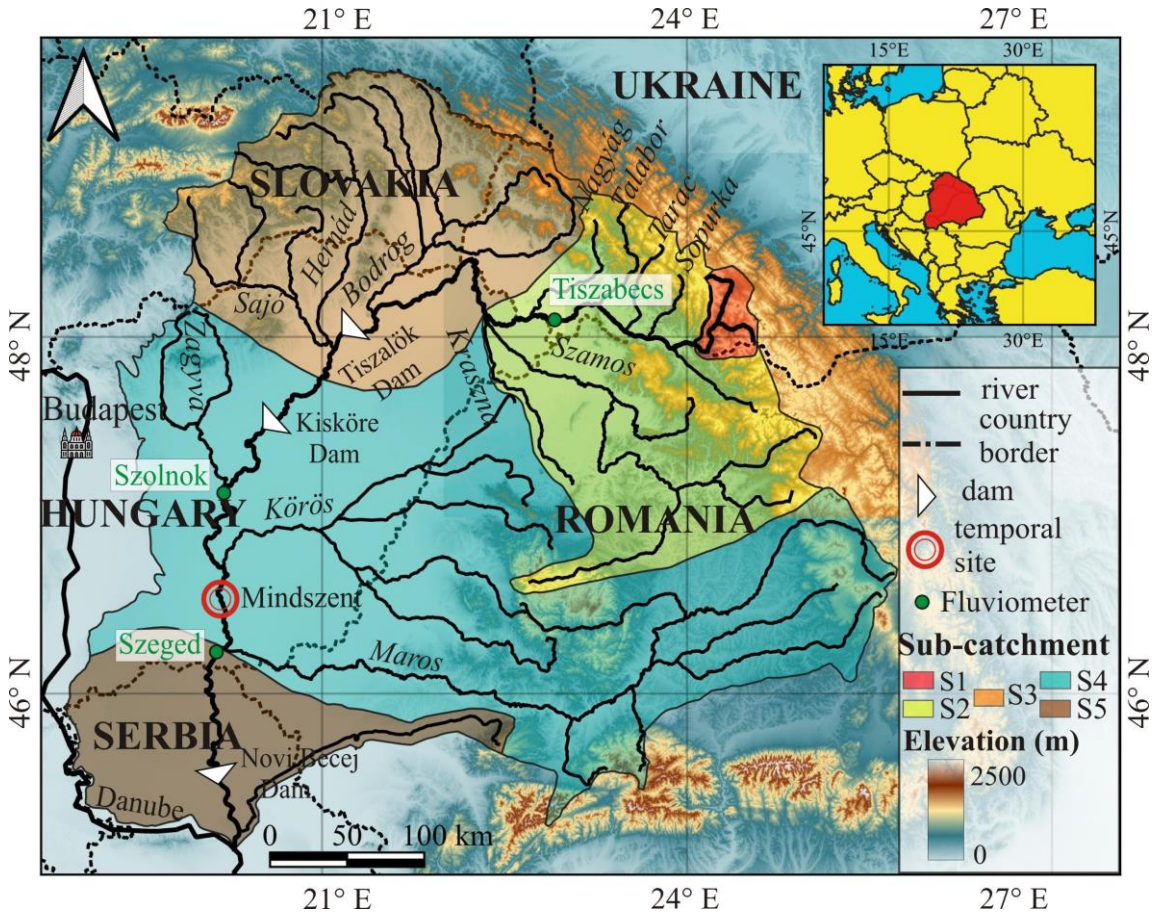

Figure 1. The Tisza River and its catchment span five European countries.

The river's topographical, morphological, and metrological characteristics divide its catchment area into three reaches (i.e., the Upper, Middle, and Lower Tisza) and five sections (i.e., S1–S5) (Figure 1). The catchment of the uppermost section (S1) of the Upper Tisza (964–688 river km; topographical head:1578 m) is in the Carpathian Mountains in Ukraine, while its downstream section (i.e., S2) is surrounded by hilly areas in Ukraine and plains in Hungary [25,26]. The Middle Tisza's (688–177 river km: topographical head: 26 m) upstream (S3) section collects the water from the hilly Transylvania and Slovakian Basins, while the catchment of the S4 section is in the hilly Romanian areas and eastern lowlands of Hungary [25,26]. Given the homogeneity of the hydro-morphological characteristics of the Lower Tisza, the entire reach was considered as one section (i.e., S5; 177–0 river km; topographical head: 6 m) [25,26]. This reach primarily drains the lowland Serbian sub-catchment.

The Tisza catchment is under the influence of a temperate continental climate, which governs the regional precipitation pattern. Specifically, the mountainous sub-catchments of the Upper Tisza receive the highest precipitation (>1000 mm/year), while it declines to 700 mm/year in the Middle Tisza and to almost half (i.e., 500 mm/year) in the Lower Tisza [25]. The west wind is the most dominant, though the Mediterranean and Eastern European air masses are also significant [27]. The mean annual temperature ranges from 8 to 11 °C, with significant spatial and temporal variations [28]. Floods in the Tisza are more likely influenced by snowmelt rather than precipitation patterns [27]. Typically, the river

experiences floods during early spring (March–April) and early summer (June–July) [29]. Apart from these periods, the river is often in prolonged low stages and occasionally experiences droughts [29]. The aridity factor (i.e., potential evaporation to precipitation) rises from <0.2 at the eastern Hungarian border to 1.4 in the Middle Tisza [30].

The hydro-meteorological characteristics of the Tisza River are likely to be influenced by climate change, with forecasting predicting warmer and drier conditions, a shift toward a Mediterranean climate, decreased annual precipitation, and an increased frequency of extreme events, including floods [28]. FehérJános [31] forecasted a 1.1 °C to 1.5 °C rise in the mean annual temperature in Tisza's catchment by 2050. Lovász [32] reported a 1.24 °C increase in the water temperature of the Danube and Tisza between 1951 and 2010, indicating significant warming, particularly during the winter months. Additionally, the groundwater table has dropped by a few meters in certain areas in the last decades due to climate change [33].

The floodplain of the Tisza is quite diverse and exhibits spatiotemporal variability. Remarkably, it includes riparian forests (e.g., willows and poplars) along the riverbanks reinforcing its stability, wetlands and marshes (e.g., reeds and sedges) providing habitat for aquatic species, and grasslands in the drier parts supporting grazing activities [34].

The downstream increase in water and sediment discharge in the Tisza is attributed to tributaries, mainly the Szamos and Kraszna in the Upper Tisza and the Bodrog, Sajó, Zagyva, Körös, and Maros in the Middle Tisza. Additionally, the river is regulated by three dams: the Tiszalök, Kisköre, and Novi Becej dams [24].

The depth of the Tisza's aquifer varies significantly across its sub-catchments, ranging from a few meters to over 100 m, depending on the geological formation [35]. The recharge rate is the highest in the mountainous sub-catchments (200–300 mm/year), while it is limited in the lowlands (50–100 mm/year) [30]. Groundwater significantly contributes to the Tisza's discharge (base flow), especially during low stages, with its contribution estimated to be about 40% in the lowlands [30].

2.2. Data Collection

The spatiotemporal dynamics of the SWT of the Tisza River and the influence of various natural and anthropogenic factors were investigated in detail based on data from 2023. This was achieved through Landsat 8 and 9 images along the river, collected monthly at specific dates and hourly in situ measurements of water temperature measured at the Szeged fluviometer. Specifically, each month, four images from the paths and rows of 185/27, 186/26, 187/27, and 187/28, covering the entire length of the Tisza, were acquired from the Copernicus open access hub (available at: https://dataspace.copernicus.eu; accessed on 20 February 2024) (Table A1). The images were obtained at level 2 and were as synchronous as possible with a timeframe of ±2.7 days. However, the timeframe was extended to ±17 days to avoid intensive cloud cover during the winter months.

Additionally, hourly in situ measurements of water temperature measured at the Szeged fluviometer (1 January 2023–31 December 2023) were obtained from the Danube Hydrological Information System website (available at: https://www.danubehis.org/; accessed on 25 February 2024). These data were used to validate the SWT satellite estimates and investigate the temporal dynamics of Tisza's water temperature throughout the year. Under ideal conditions, the TIRS sensor onboard Landsat 8 and 9 estimates land surface temperature with a high rate accuracy of ±1–2 °C. However, in narrow channels, the presence of riverbanks can affect estimation accuracy due to the occurrence of mixed pixels. To assess this impact on the Tisza River, different channel sections of varying widths were tested. Since the channel size of the Tisza increases toward the downstream area (mean of the Upper Tisza: 50 m, Middle Tisza: 150 m, and Lower Tisza: 250 m [23]), additional in situ measurements of water temperatures measured in the Upper Tisza (at Tiszabecs) and Middle Tisza (at Szolnok) (Figure 1) were obtained to further validate the satellite estimates. Notably, these three sites are sufficient to assess the influence of river size on the estimation accuracy of SWT and are comparable to the validation dataset size applied in

the literature [2,36–38]. To evaluate the impact of seasonal variations in water stage/discharge and consequently channel width, the strength of the correlation between water stage and the difference in SWT estimated by satellites versus in situ measurements was calculated across the three measurement sites. To evaluate the influence of climate change on the SWT of the Tisza, the thermal bands of 438 Landsat 4, 5, 7, 8, and 9 covering the Mindszent site (Figure 1; path 187 or 186 and raw 28) between 13 June 1984 and 27 January 2024 were analyzed. This site was selected because it is located between two tributaries, and no large-scale human impact affects the thermal conditions of the river. The images were explored in Google Earth Engine (GEE), especially the collection 2 Tier 1 dataset for Landsat 4, 5, and 9 and the collection 2 Tier 1 and real-time datasets for Landsat 7 and 8.

While the TM sensor in Landsat 4 and 5 records thermal emissions in a single band (i.e., B6; 10.4–12.5 μm) with a spatial resolution of 120 m, the ETM+ sensor in Landsat 7 records the emissions in low and high gain bands (i.e., B6L and B6H; 10.4–12.5 μm) with a finer spatial resolution of 60 m. On the other hand, Landsat 8 and 9 carry separate sensors for thermal emissions (i.e., TIRS), providing thermal data in two bands (i.e., B10: 10.6–11.19 μm and B11: 11.50–12.51 μm) with a 100 m spatial resolution. Notably, the B6H in Landsat 7 and B10 in Landsat 8 and 9 were used in this study. Given the variability in the spatial resolution of the thermal bands in the Landsat satellites, they were resampled to 30 m for uniformity purposes.

2.3. Processing of Satellite Images

All Landsat images were obtained at level 2 (surface reflectance/temperature), meaning that they were already radiometrically, geometrically, and atmospherically corrected [39]. Radiometric correction aimed to convert the digital number (DN) to at-sensor radiance (Equation (1)) [2], allowing for comparative analysis of satellite data over time and across sensors. To accommodate the influence of atmospheric scattering and absorption, the at-sensor radiance is typically corrected by radiative transfer models for Landsat 4, 5, and 7 and by the Landsat surface reflectance code (LaSRC) for Landsat 8 and 9. Planck's equation was applied to retrieve the SWT (Equation (2)) [2]. Finally, the SWT was converted from Kelvins (K) to Celsius (°C) (Equation (3)).

$$L_\lambda = DN \times gain + bias \quad (1)$$

where L_λ is the at-sensor radiance (W/m²/sr/μm) and $gain$ and $bias$ are sensor-based calibration parameters.

$$T_s = \frac{K_2}{\ln\left(\frac{K_1}{L_{\lambda(T_S)}}+1\right)} \quad (2)$$

where T_s is the surface water temperature (K), $L_{\lambda(T_s)}$ is the atmospherically corrected water surface radiance, and K_1 and K_2 are sensor-based thermal constants.

$$T_k = T_c + 273.1 \quad (3)$$

where T_k is the temperature in Kelvins and T_c is the temperature in Celsius.

To explore the thermal profile of the entire Tisza, the four monthly Landsat 8 and 9 images were mosaicked. The raster geometric mosaic tool in SNAP (ESA) V10.0.0 software was utilized to mosaic the images. The final pixel value in overlapping regions was determined using a weighted average algorithm, where the weights are typically based on the distance of each pixel from the center of the overlap. Since the images cover a large scale of the river, there is a high probability of cloud occurrence. Thus, the clouds were masked using the pixel quality assessment band (i.e., the qa_pixel band) provided by the CFMASK algorithm [40]. Then, the pure water pixels of the river were extracted by applying the Normalized Difference Water Index (NDWI), which relies on the green and near-infrared bands [41]. The threshold of the index was automatically selected by the Otsu algorithm [42], which resulted in threshold values of 0.01, 0.05, 0.1, and 0.02 for the four mosaicked images. To overcome the occurrence of mixed pixels that may originate from the

application of the NDWI multispectral-based water mask (high spatial resolution) to the thermal band (low spatial resolution), strict threshold values were selected. Additionally, the water mask was calculated based on images from August when the water stage is the lowest (i.e., the narrowest water width), and this mask was then applied to the rest of the images. By doing so, a significant portion of mixed pixels could be avoided. The centerline of the river was identified, and the SWT was estimated every 2 km along the centerline. All processing steps of the satellite images were implemented in SNAP (Sentinel Application Platform) V10.0.0 software [43].

2.4. Data Analysis

To verify the accuracy of Landsat SWT estimates in the medium-sized Tisza River, the Landsat-based SWT estimates at specific dates every month were compared with in situ water temperature data measured in the Upper (i.e., Tiszabecs), Middle (i.e., Szolnok) and Lower (i.e., Szeged) Tisza. Remarkably, the in situ measurements are available hourly, resulting in only a half-hour time difference between the measured and estimated SWT. The difference in the acquisition dates of the mosaicked images was considered. Thus, the satellite-based SWT estimates at any given measuring site on a specific day were compared to their corresponding in situ measurements taken on the same day, with just an hour difference between their acquisition times. The hourly water temperature measurements in the lower Tisza at Szeged were used to reveal the daily cycle of water temperature and its seasonal variation. This was achieved by calculating the mean hourly water temperature for each month.

Monthly thermal maps representing the thermal profile of the entire Tisza were produced (based on Landsat 8 and 9 images acquired on specific dates). These maps were used to discern the thermal trend and SWT variability along the river sections (i.e., S1–S5; Figure 1). They were also employed to reveal the influence of dams and tributaries on the thermal profile of the river and its seasonal variability. This was achieved by comparing SWT (average of 3 × 3 pixels) just downstream and upstream of their locations each month. Additionally, the SWT every 30 m for 2 km channel sections upstream and downstream of the three dams in the Tisza were estimated and revealed.

To demonstrate the potential of Landsat satellites in detecting thermal plumes from wastewater treatment plants (WWTPs) in a medium-sized river, the locations of six WWTPs in the Middle and Lower Tisza were compared to the monthly thermal maps. Also, the SWT (average of 3 × 3 pixels) difference between the downstream and upstream areas of the effluents was calculated.

Finally, the SWT at the Mindszent site (the average of 3 × 3 pixels) over the last 40 years was calculated, and the Mann–Kendall trend analysis test [44,45] was applied to investigate the influence of climate change on the water temperature of the Tisza. All statistical analyses were implemented using Microsoft Excel 365, SPSS V 26.0 software, and Python [46].

3. Results

3.1. Validity of Landsat Surface Water Temperature (SWT) Estimates

Generally, the Landsat 8 and 9 satellites provided high estimation accuracy of SWT for the three tested sites in the Upper, Middle, and Lower Tisza (Figure 2A), since it gave an elevated R^2 of 0.94 and a low RMSE of 3.66 °C. However, when considering individual sites, the best estimates were observed in the Lower Tisza at Szeged ($R^2 = 0.99$; RMSE = 1.43 °C; Figure 2D), while the worst estimates were in the Upper Tisza at Tiszabecs ($R^2 = 0.92$; RMSE = 4.73 °C; Figure 2B). Remarkably, the Landsat estimates tend to overestimate the SWT, particularly during the summer months (e.g., July and August), while it tends to slightly underestimate it during winter months (e.g., December and January). Additionally, the magnitude of underestimation or overestimation increases with decreasing channel size. Seasonal variations in water discharge and the consequent changes in river

width have a significant influence on satellite-based SWT estimation. This is evidenced by the strong negative correlation of −0.6 between the water stage and the difference between measured and estimated SWT across the three stations.

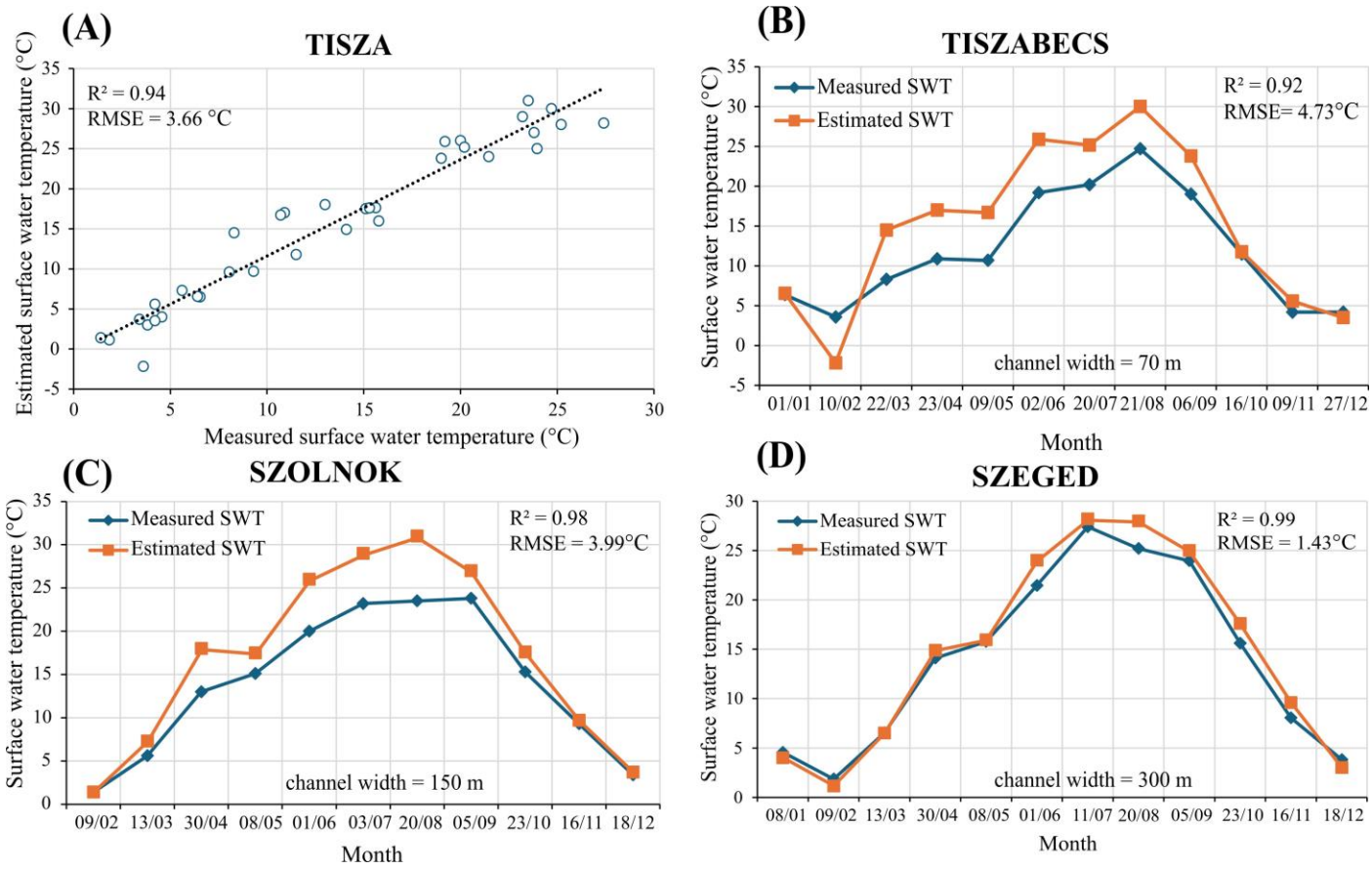

Figure 2. Evaluation of the Landsat 8 and 9 surface water temperature (SWT) estimates in the Tisza River (**A**), and at specific sites in the upper (at Tiszabecs) (**B**), middle (at Szonlok) (**C**), and lower (at Szeged) (**D**) reaches of the river.

3.2. Water Temperature in the Tisza River and Its Daily Cycle (In Situ Data)

The mean water temperature in the Tisza River at Szeged in 2023 was 14.10 ± 8.46 °C, with seasonal averages of 3.93 ± 0.91 °C in winter, 11.33 ± 4.19 °C in spring, 24.48 ± 1.61 °C in summer, and 16.69 ± 5.65 °C in autumn. The hottest month was July (25.80 ± 0.18 °C), while the coldest was February (2.94 ± 0.06 °C) (Figure 3).

Based on the mean water temperature measured hourly, the daily cycle of water temperature in the Tisza varies significantly across different months (Figure 3). Notably, the highest difference in water temperature between day and night occurred during the summer months, particularly in July (0.53 °C), while the lowest difference was observed in winter, especially in January (0.07 °C). Although this temperature difference is relatively low in spring and autumn, a notable increase was observed in March (0.31 °C) and November (0.30 °C).

Additionally, the timing of minimum and maximum water temperature throughout the day varied across the months (Figure 3). Typically, the minimum temperature occurred around 7:00 to 8:00 in winter and spring, shifting to 9:00 to 10:00 in summer and autumn. An exception was March, November, and December when the minimum temperature occurred around 23:00 to 00:00. The timing of the maximum temperature showed greater seasonal variability, occurring around 14:00 to 16:00 in winter, 17:00 to 19:00 in spring, 19:00 to 20:00 in summer, and 00:00 to 01:00 in autumn.

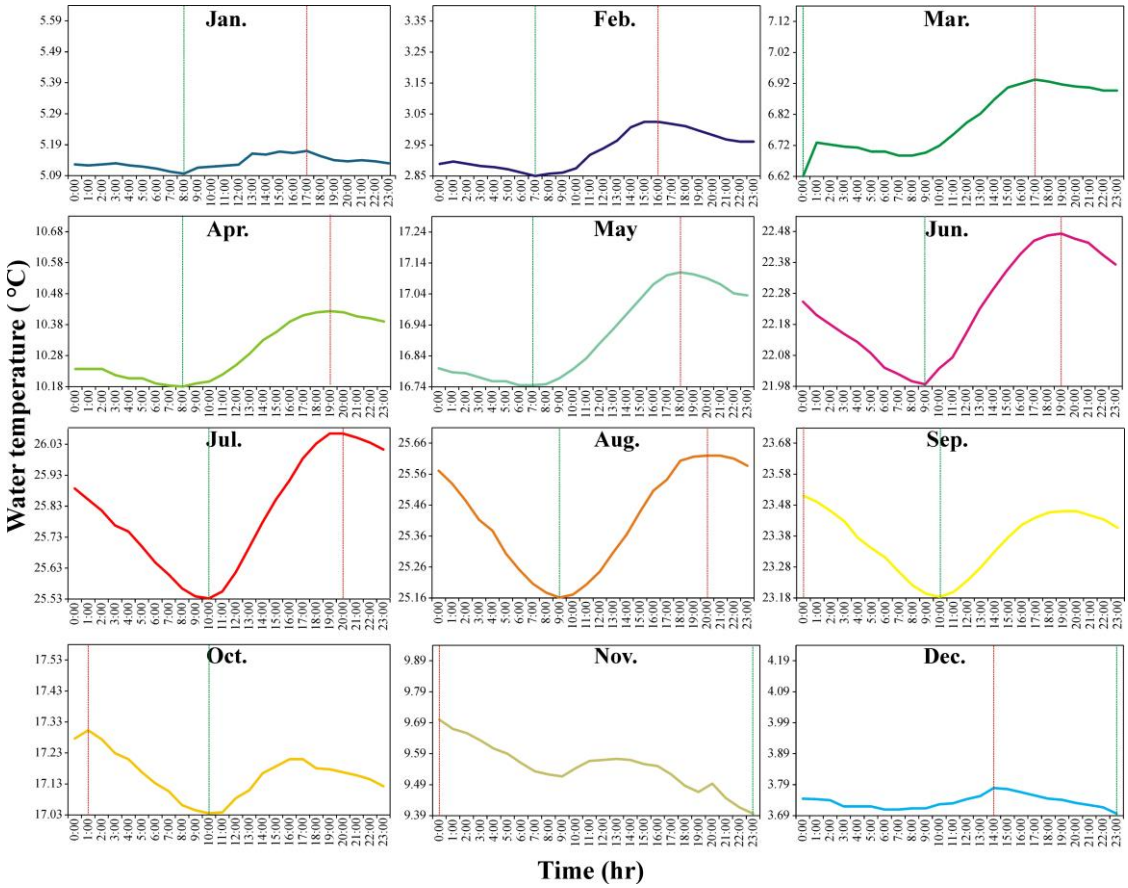

Figure 3. The monthly mean hourly water temperature in the Tisza River (at Szeged) in 2023.

3.3. Longitudinal Thermal Profile of the Tisza River (Satellite Data)

The satellite estimates of SWT every 2 km along the Tisza were averaged to reveal the monthly longitudinal thermal profile of the river at the section scale (i.e., S1–S5) in 2023 (Figure 4). Aligning with in situ measurements of water temperature (at Szeged), the satellites indicated August and July as the hottest months and February as the coldest month. The thermal profile of the river varied across the months with a decreasing trend, toward the downstream area in January–April, June, August, and September, and an increasing trend in the remaining months. However, the mean SWT profile indicated a slight overall increasing trend downstream. In the meantime, if the upper sections (i.e., S1 and S2) are excluded due to the elevated uncertainty of SWT estimation given the narrow and shallow channel, an increasing trend occurred in most months, including January–February, April, July, and September–November, with a general increasing trend in the mean.

Based on the annual mean profile, the first section (S1) was the warmest (15.48 ± 1.89 °C), while the third section (S3) was the coldest (14.55 ± 1.16 °C) (Figure 4). However, if the upper sections are excluded, section S5 was the warmest section (15.43 ± 0.73 °C), and section S3 is still the coldest. Remarkably, the variability in SWT was the highest in the upper sections (standard deviation in S1: ± 1.89 °C and S2: ± 1.99 °C), while it declined gradually, recording its lowest level in the lower section (S5: ± 0.73 °C). The mean difference in SWT between the sections was 2.81 ± 0.83 °C, though it surged to 6.84 ± 0.69 °C in February–March and October–November. By excluding the upper sections (i.e., S1 and S2), the mean SWT difference declined to 1.64 ± 0.99 °C, though it was still high (i.e., 4.28 ± 2.10 °C) in February–March and October–November.

Since the longitudinal thermal profile of the river at the section scale obscures local changes, it was also depicted at a 2 km scale (Figure 5). A significant variation in SWT was noticed in the Upper Tisza (S1 and S2), especially in the summer, declining gradually,

toward the downstream area. However, these intensified variations are likely attributed to narrow and shallow channels, along with the appearance of bars during low stages in summer (Figure 6A). These factors affect the thermal emission of water pixels by the surrounding riverbanks and/or bars. This was also observed in some channel sections in the Middle and Lower Tisza, particularly in meandering sections, though with lower magnitudes (Middle Tisza: Figure 6B; Lower Tisza: Figure 6C).

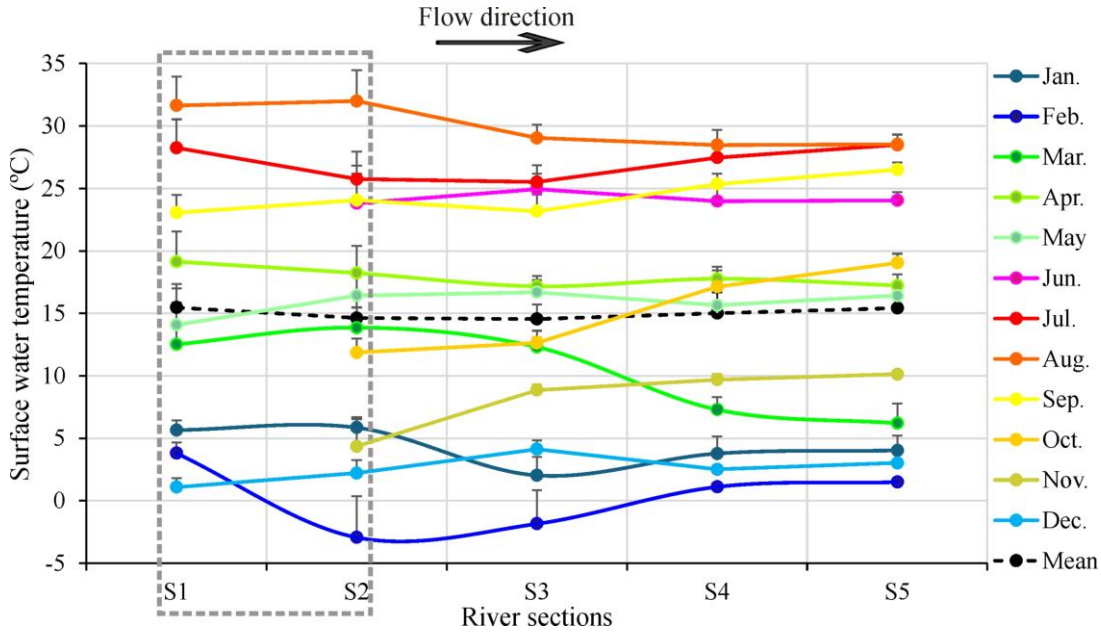

Figure 4. Monthly longitudinal thermal profile of the Tisza River at the section scale (S1–S5) in 2023. The monthly SWT data are based on satellite estimates on a specific date each month (Table A1). The gray dotted box refers to sections with narrow and shallow channels, resulting in low SWT estimation accuracy (interpret with caution).

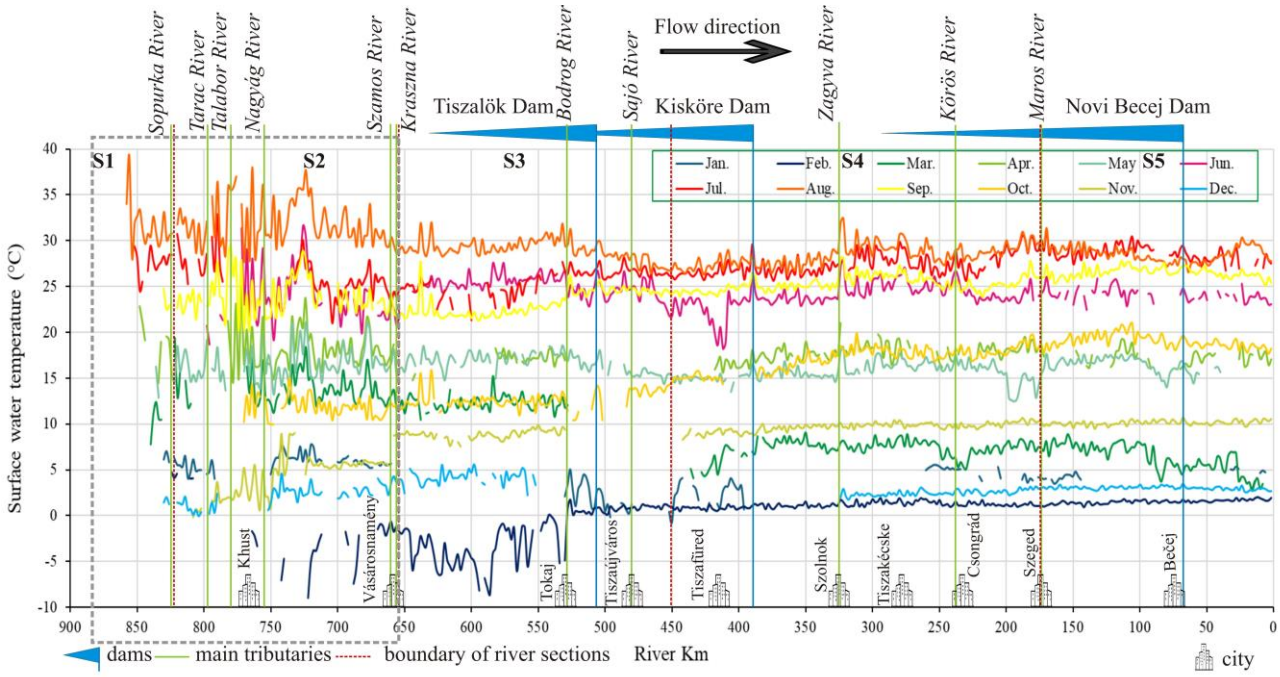

Figure 5. Monthly longitudinal thermal profile of the Tisza River at a 2 km scale in 2023, including the locations of the main tributaries, dams, and cities. The monthly SWT data are based on satellite estimates on a specific date each month (Table A1). The gray dotted box refers to sections with narrow and shallow channels, resulting in low SWT estimation accuracy (interpret with caution).

Channel sections in close vicinity to towns (e.g., Szeged, Szolnok, and Tiszakécske) are usually associated with elevated SWT, especially during the summer and spring, while it declines in winter and autumn (Figures 5 and 6D–F). Considering the ten main towns located along the Tisza River (Figure 5), Szolnok showed the greatest increase in SWT in the adjacent channel section, particularly between January and July (Figures 7 and A1). A significant increase in SWT also occurred in the channel sections by Szeged and Tiszakécske, while the lowest impact was observed at Vásárosnamény (Figures 7 and A1).

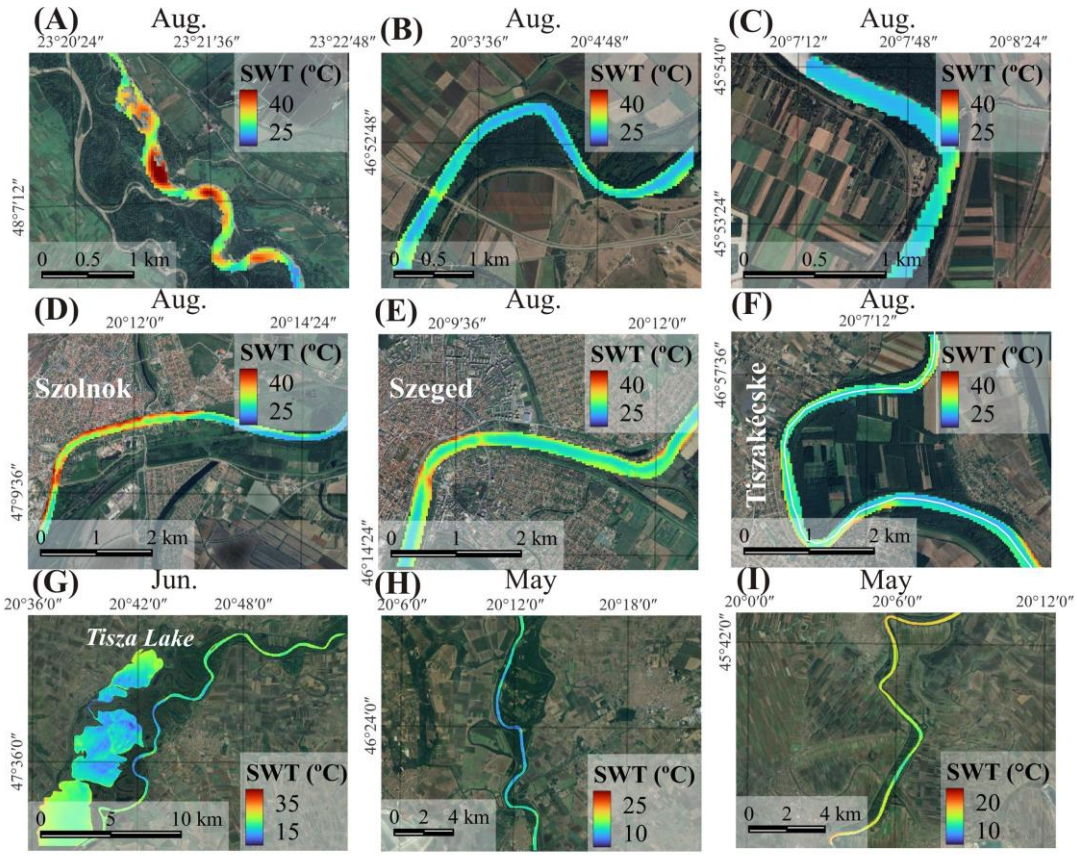

Figure 6. Examples of overestimated surface water temperatures (SWT) at meandering and narrow channel sections in the Upper (**A**), Middle (**B**), and Lower (**C**) Tisza. The influence of selected cities located along the Tisza River in Hungary on SWT in adjacent channel sections (**D**–**F**). A decline in SWT was observed in some channel sections in the Middle (**G**,**H**) and Lower (**I**) Tisza.

Remarkably, some channel sections exhibited a sudden decline in SWT (Figure 5), and the magnitude of this decline varied across the months, with higher declines in spring and summer than in winter and autumn. For instance, the 20–22 river km (Figures 5, 6I and A2C) and 80–84 river km (Figures 5, 6H and A2B) channel sections usually exhibit a decline in SWT profile across the months, with significant declines of 0.7 °C and 2.8 °C in May, respectively. Notably, the SWT also declined profoundly by 6.1 °C in the 406–422 river km channel section (Figures 5 and 6G), along the Tisza Lake impounded by the Kisköre Dam, but only in June.

After comparing the locations of the six main WWTPs in the Middle and Lower Tisza with the monthly thermal maps and calculating the temperature difference between the downstream and upstream areas of their effluents, no or just a slight increase was noticed for most WWTPs. This may indicate their limited impact, which could not be captured by the relatively coarse spatial resolution Landsat TIR sensor (pixel size: 100 m). Additionally, the complexity of factors influencing the thermal profile of rivers may interfere with the WWTP's influence, hindering differentiation between their specific effects.

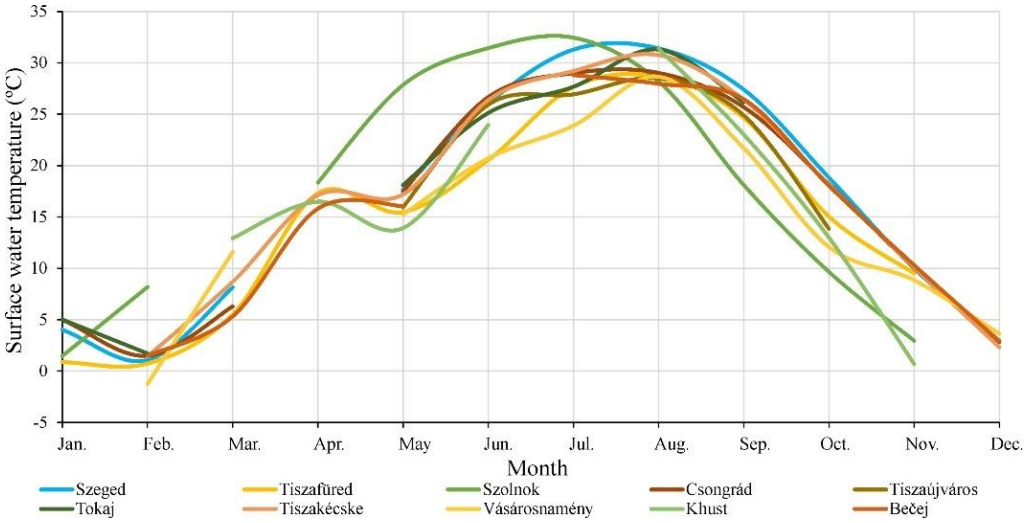

Figure 7. Monthly surface water temperature (SWT) at channel sections adjacent to eight towns in Hungary located along the Tisza River in 2023. The missing data refer to cloudy images. The monthly SWT data are based on satellite estimates at a specific date each month (Table A1). The interpretation of SWT in the channel section next to Khust should be conducted with caution, owing to its narrow width and low estimation accuracy.

3.4. Influence of Tributaries and Dams on the Thermal Profile of the Tisza River

The influence of tributaries on the SWT of the Tisza varied, with a likely increase in 75% of cases (Figures 5 and 8). Each tributary exhibited different influences across the months, except for the Bodrog River, which shows a consistent increase in SWT throughout the year. Remarkably, the magnitude of increase or decrease is more pronounced in spring and summer compared to winter and autumn. The highest absolute difference was 3.36 °C in Zagyva River, recorded in June, while the lowest absolute difference was 0.012 °C in Maros River, recorded in February. The Sajó, Zagyva, Körös, and Maros rivers typically decrease the SWT of the Tisza in winter and autumn, while they increase it during the rest of the year. On the other hand, the Szamos River decreases the SWT in winter and spring, and the Kraszna River decreases the SWT in spring and autumn, while both increase it during the remaining months.

SWT difference upstream and downstream of main tributaries

	Szamos			Kraszna			Bodrog			Sajó			Zagyva			Körös			Maros		
	US	*DS*	*Diff.*	*US*	*DS*	*Diff.*	*US*	*DS*	*Diff.*	*US*	*DS*	*Diff.*	*US*	*DS*	*Diff.*	*US*	*DS*	*Diff.*	*US*	*DS*	*Diff.*
Jan.							4.2	5.0	↑ 0.8	0.1	-0.9	↓ -0.9				4.8	5.3	↑ 0.5	4.0	5.2	↑ 1.2
Feb.	-1.2	-1.3	↓ -0.2	-1.2	-1.2	↑ 0.0	-1.8	-0.1	↑ 1.7	0.9	1.0	↑ 0.1	1.6	1.5	↓ -0.1	1.1	1.1	↓ -0.1	1.0	1.0	↓ 0.0
Mar.	12.2	12.4	↑ 0.2	11.6	11.2	↓ -0.4							7.5	7.9	↑ 0.3	5.1	5.4	↑ 0.4	7.4	7.5	↑ 0.1
Apr.	17.7	17.3	↓ -0.4				16.8	17.8	↑ 1.0				20.0	20.7	↑ 0.7	16.9	17.8	↑ 0.9	18.1	18.4	↑ 0.3
May	16.5	16.5	↓ 0.0				17.1	18.0	↑ 0.9	15.1	15.8	↑ 0.8	17.8	19.6	↑ 1.8	15.5	16.4	↑ 0.9	14.9	15.6	↑ 0.6
Jun.	22.3	22.9	↑ 0.6	20.3	21.7	↑ 1.4	24.9	26.3	↑ 1.5	24.4	24.6	↑ 0.2	26.9	30.3	↑ 3.4	23.7	24.8	↑ 1.1	24.1	24.9	↑ 0.8
Jul.	24.1	24.8	↑ 0.7	24.3	24.7	↑ 0.4	28.4	29.5	↑ 1.2	26.4	26.5	↑ 0.2				25.8	27.2	↑ 1.3	29.4	29.1	↓ -0.3
Aug.	28.9	30.1	↑ 1.3	28.7	28.9	↑ 0.3	30.7	32.0	↑ 1.3	28.8	28.2	↓ -0.6	30.9	32.9	↑ 2.0	27.7	28.5	↑ 0.8	29.9	30.5	↑ 0.6
Sep.	22.0	22.9	↑ 1.0	21.7	21.6	↓ 0.0	22.7	25.7	↑ 3.1	24.8	24.7	↓ -0.1	27.8	30.3	↑ 2.6	24.8	24.7	↓ -0.1	26.9	25.6	↓ -1.3
Oct.	11.9	12.6	↑ 0.7	12.1	12.2	↑ 0.1				13.8	13.8	↑ 0.0	18.5	18.8	↑ 0.3	17.4	17.5	↑ 0.1	18.6	18.3	↓ -0.4
Nov.	9.4	8.9	↓ -0.5	8.9	9.1	↑ 0.1							10.0	9.7	↓ -0.3	9.3	9.9	↑ 0.6	10.3	10.0	↓ -0.3
Dec.	4.1	3.8	↓ -0.4	3.7	4.1	↑ 0.4							1.9	2.1	↑ 0.2	2.5	3.0	↑ 0.5	3.0	3.0	↑ 0.0

US: upstream DS: Downstream Diff.: difference ↑ SWT increase ↓ SWT decrease

Figure 8. Monthly influence of the main tributaries on the thermal profile of the Tisza River in 2023. The monthly SWT data are based on satellite estimates on a specific date each month (Table A1).

Based on the detailed SWT data (estimated every 30 m) for 2 km long channel sections upstream and downstream of the three dams in the Tisza (i.e., the Tiszalök, Kisköre, and Novi Bečej dams), a sudden SWT change typically occurs at each dam (Figures 5 and 9). This change is more pronounced in spring and summer than in autumn and winter. Remarkably, the three dams showed slightly different thermal patterns. Specifically, while the Kisköre and Novi Bečej dams tend to cause a sudden increase (mean increase at Kisköre Dam: 0.65 ± 1.13 °C; Novi Bečej Dam: 0.5 ± 1.2 °C) just upstream of the dam, in its reservoir, and a sudden decrease (mean of Kisköre Dam: 0.66 ± 1.32 °C; Novi Bečej Dam: 0.48 ± 1.3 °C) downstream of the dam, the SWT of the channel section upstream of the Tiszalök Dam was usually high, with the dam causing a sudden decline downstream (mean: 0.55 ± 0.62 °C). The thermal profile rarely declined at the channel section of a dam, and this occurred only once in March at the Kisköre Dam, though a sudden SWT change was also recorded at the location of the dam (Figure 9B).

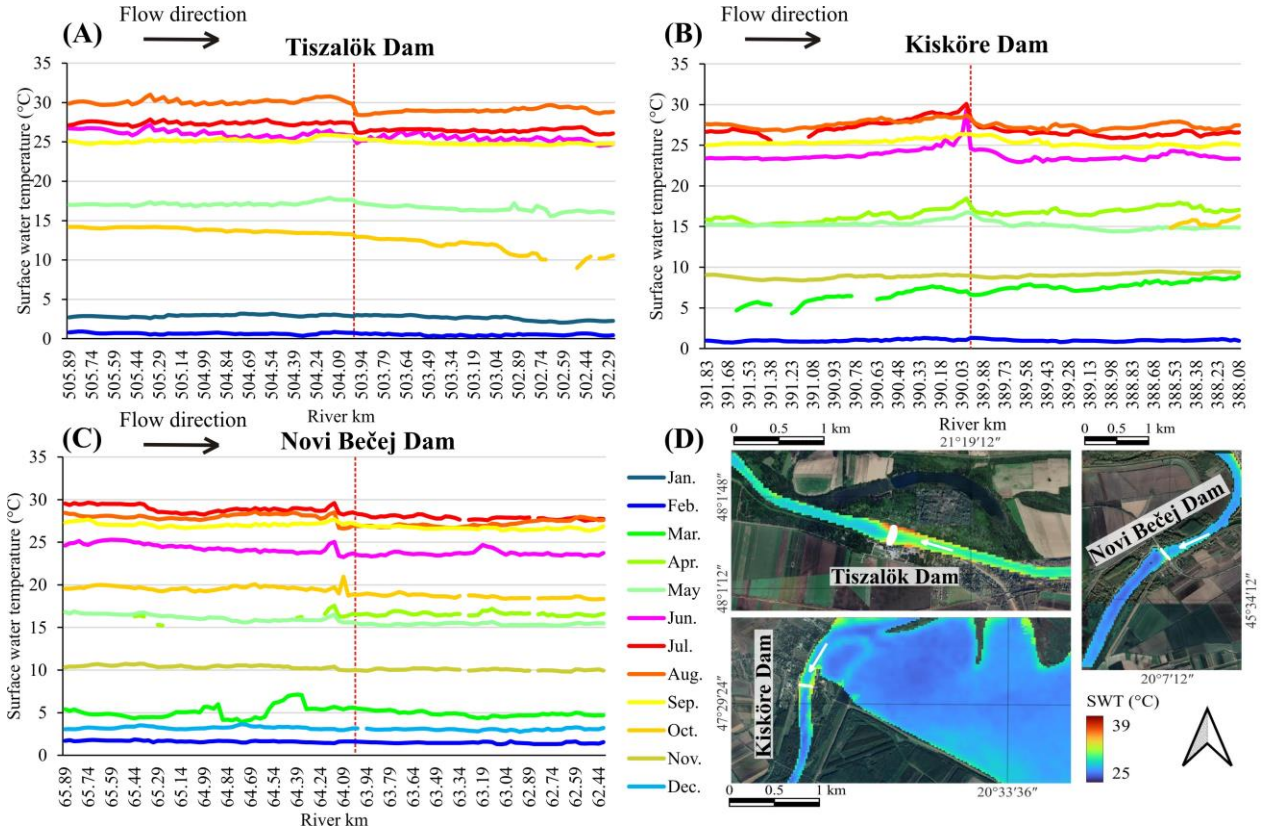

Figure 9. Monthly thermal profile of 2 km river channel sections upstream and downstream of the Tiszalök (**A**), Kisköre (**B**), and Novi Bečej (**C**) dams in the Tisza River, based on SWT data obtained by the Landsat TIR sensor every 30 m in 2023. Examples of Landsat-based SWT upstream and downstream of the three dams of the Tisza in August 2023 (**D**). The monthly SWT data are based on satellite estimates on a specific date each month (Table A1).

3.5. Influence of Climate Change on the Surface Water Temperature of the Tisza River (40 Years of Satellite Data)

Based on 438 Landsat images between 13 June 1984 and 27 January 2024, a time series of SWT and the mean annual SWT in the Tisza River at the Mindszent site are depicted (Figure 10). Throughout this period, the lowest SWT was –5.71 °C, recorded on 28 December 1992, and the highest was 32.83 °C, recorded on 17 March 2010, with a mean SWT of 14.57 ± 7.83 °C and a mode of 21.43 °C (Figure 10A). The mean annual SWT of data revealed that the year 1996 was the coldest (7.39 ± 8.66 °C) and the year 2003 was the hottest (22.70 ± 1.30 °C) (Figure 10B). The Mann–Kendall trend analysis test indicated a significant increasing trend in SWT during the study period (Z-value = 1.689 and *p*-value = 0.091),

with an annual increasing rate of 0.068 °C, resulting in a total rise of 2.74 °C over the monitoring period at this temporal monitoring site.

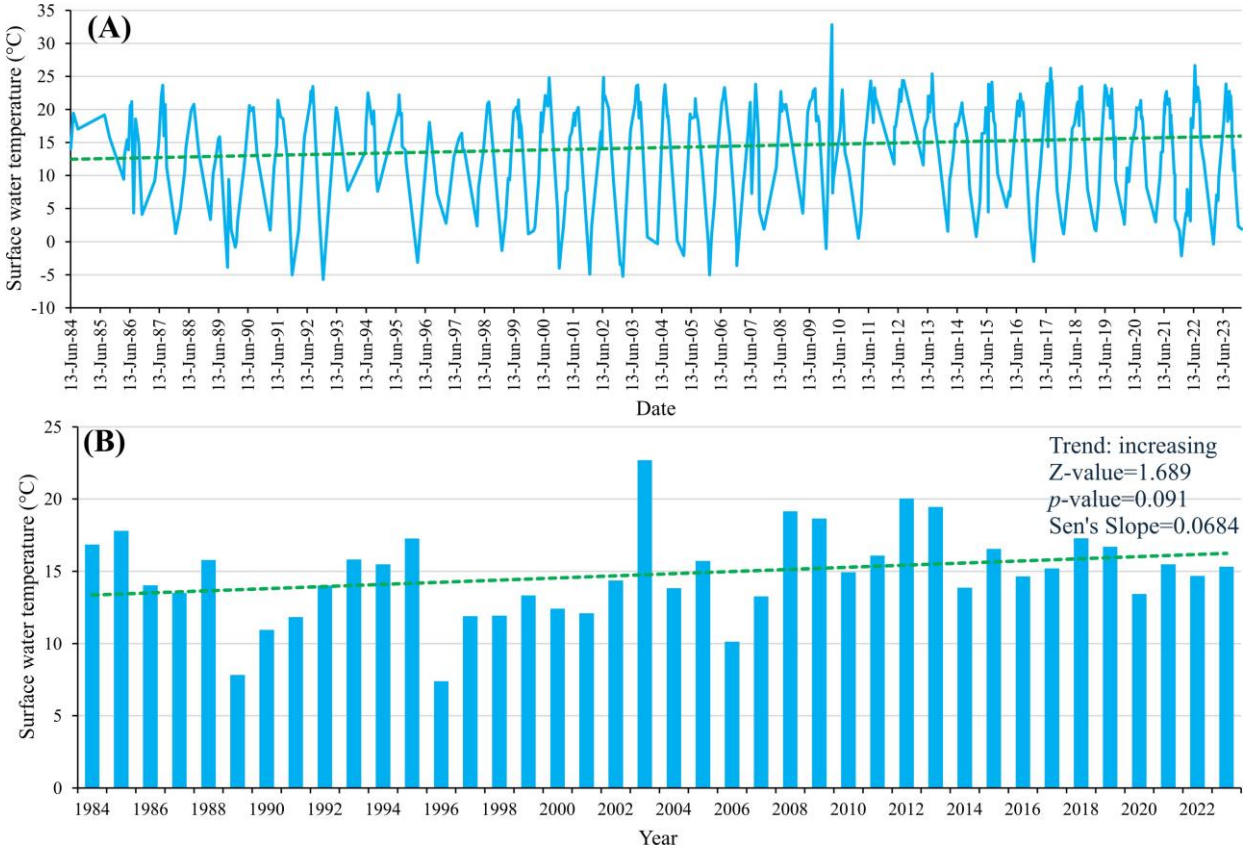

Figure 10. Time series of surface water temperature (SWT) in the Tisza River at Mindszent between 13 June 1984 and 27 January 2024 based on 438 Landsat satellite images (**A**). Mean annual SWT during the studied period (1984 to 2024) (**B**).

4. Discussion

The thermal characteristics of riverine systems are crucial for water quality conditions and ecological health; however, their spatiotemporal dynamics remain understudied due to insufficient monitoring systems. This study provides a comprehensive assessment of various natural and anthropogenic factors influencing the thermal profile of the Tisza River in Central Europe, employing Landsat satellite images and in situ water temperature measurements. The results demonstrate the degree of efficiency of satellite-based SWT estimation and its suitability for evaluating factors at varying scales. Additionally, the study offers critical insights into the variability of Tisza's thermal profile across multiple spatiotemporal scales in response to these driving factors.

4.1. Assessment of Landsat Thermal Bands for Surface Water Temperature Evaluation of a Medium-Sized River (Tisza River)

The Landsat satellites provided valuable real-time, free, and large-scale thermal data for evaluating the thermal profile of the Tisza River across multiple spatiotemporal scales. The TIRS sensor onboard Landsat 8 and 9 has an absolute radiometric accuracy of better than 5% uncertainty (TOA radiance), enabling it to estimate land surface temperature with a high level of accuracy (±1–2 °C) [47]. However, this accuracy level could be influenced by the size and morphological and hydrological conditions of the river, which resulted in an additional ±1.66–2.66 °C of uncertainty in the estimated SWT in the Tisza, based on the three tested sites (R^2 = 0.94; RMSE = 3.66 °C). This accuracy is comparable to Landsat-based SWT estimations in the Łebsko and Gardno lakes, Poland (R^2 = 0.95) [36], and in the

Embalse del Río Tercero reservoir, Argentina ($R^2 = 0.95$) [37]. However, it is slightly lower than the reported accuracy for the Han River, China ($R^2 = 0.97$) [2], which may be attributed to the narrower channel size of the Tisza River (mean width: 150 m) compared to the Han River (mean width: 450 m). Given the significant variability in channel morphology, size, hydrology, and local environmental conditions along the Tisza's sections, the uncertainty of SWT varied. The highest confidence was achieved in the lower sections where the channel is wide and deep whereas the confidence decreased toward the upper sections with shallow and narrow channels coupled with bars, islands, and less stable flow conditions. Also, the estimation accuracy is influenced by fluctuations in flow conditions, affecting channel width with higher confidence during high stages (wider channels) compared to low stages (narrower channels). Based on the evaluation of a diverse array of satellites and airborne platforms, Handcock, et al. [18] reported that the estimation accuracy of SWT significantly declines when the pure water of the river channel is resolved by less than three pixels. This explains the higher RMSE of 4.73 and 3.99 °C in the Upper and Middle Tisza with a channel width of 70 and 150 m (i.e., 0.7 and 1.5 pixels), respectively, while it declined to 1.43 °C in the Lower Tisza with a channel width of 300 m (i.e., 3 pixels). This systematic error can largely be eliminated if the goal is to estimate relative SWT between two sections or within a specific timeframe at a given location.

Additionally, the resulting thermal maps could not accurately detect the influence of WWTPs on the thermal profile of the Tisza. This limitation can be attributed to the coarse spatial resolution of the thermal band and the localized impact of WWTP effluents.

On the other hand, cloud cover and the relatively long revisit time of Landsat satellites (16 days) lead to incomplete thermal data and the mosaicking of non-synchronous images. For instance, the mean timeframe difference between the four mosaicked images covering the entire Tisza reached ± 17 days in winter and autumn, which resulted in discontinuous thermal data, and inaccurate evaluation of the thermal profile of the large-scale Tisza River. However, it is still beneficial for assessing individual reaches. This issue may be responsible for the elevated SWT difference of 6.84 ± 0.69 °C between the five sections or 4.28 ± 2.10 °C between the last three sections (i.e., S3–S5) in February–March and October–November, which are characterized by intensified cloud cover and highly non-synchronous images (Figure 4). Remarkably, even for a single reach of the river, cloud cover and long revisit time can prevent conducting a comparative analysis of thermal data across months and seasons.

4.2. Diurnal Temperature Cycle Dynamics in the Tisza River Throughout the Year

The hourly in situ measurements of water temperature in the Tisza River at Szeged in 2023 revealed strong monthly thermal variability driven by solar radiation and atmospheric conditions. In particular, the water temperature difference between day and night is the highest in summer, gradually decreasing in spring and autumn, until reaching the lowest values in winter. Also, the timing of minimum and maximum temperatures typically shifts toward later hours of the day, gradually moving from winter and spring to the latest hours in summer and autumn. These variations result from changes in solar radiation, ambient air temperatures, cloud cover, river flow, environmental conditions, and analemma effect across months. For instance, increased solar radiation, low flow rate, and long daylight hours in summer lead to longer exposure of river water to heating compared to the low solar radiation, high flow rate, and short daylight hours in winter. This results in significant diurnal temperature variations across the months. A similar finding was reported by Niedrist [48] in two mountainous rivers in Central Europe (i.e., the Inn and Grossache rivers).

4.3. Spatiotemporal Dynamics of the Thermal Profile of the Tisza River at the Section Scale

The monthly Landsat-based thermal profiles of the Tisza revealed a generally uniform profile with a slightly increasing trend, toward the downstream area, though significant variations were noticed across the months (Figures 4 and 5). This thermal profile

aligns with those of other lowland rivers worldwide with low water heads [7]. Notably, the asymptotic downstream increasing trend is a common longitudinal thermal profile of many river systems [7]. This pattern results from the interplay of high precipitation and snowmelt rates, groundwater inflow, and the availability of riparian shading in headwaters, which cool the waters in these reaches compared to downstream sections. On the other hand, a general decreasing trend was also noticed in some months, particularly in summer (e.g., June and August). This could result from reduced water volume, flow rate, and mixing in headwaters, leading to warmer water compared to downstream reaches. Additionally, a complex thermal profile was observed in other months (e.g., January and February), showing sudden drops in some sections. These anomalies could be attributed to local natural and/or anthropogenic factors affecting these reaches during these particular months. In the meantime, the elevated SWT uncertainty in small-sized channel sections and long timeframe differences between mosaicked images could also be the main causes of such complex patterns. Therefore, the interpretation of the Landsat-based thermal profile of a medium-sized river like the Tisza, with varying channel sizes and flow conditions, should be conducted with caution.

4.4. Spatiotemporal Dynamics of the Thermal Profile of the Tisza River at a 2 km Scale

The detailed thermal profile of the Tisza (SWT every 2 km) revealed thermal anomalies primarily located in urban areas, dams, tributaries, and meandering sections, with more pronounced magnitudes in summer and spring compared to winter and autumn (Figures 5, 8 and 9). This underscores the significant influence of urban heat islands, thermal impacts from natural and anthropogenic activities, and geographical features on the thermal profile of the Tisza. Aligning with the literature, the drivers and magnitudes of these anomalies varied across different landscapes of the river system and seasonally, owing to variability in solar radiation, flow discharge, and thermal inertia [7,49].

4.4.1. Influence of Urban Areas

Interestingly, the thermal influence of urban areas showed a strong association with prevailing anthropogenic activity and population density. For instance, Szolnok and Szeged showed the highest increase in SWT in nearby channel sections, linked to industrial activities and high population density (Szeged: 612.3 inhabitants/km^2; Szolnok: 129 inhabitants/km^2) [50]. Despite Tiszakécske having a relatively low population density (58 inhabitants/km^2) [50], it also showed remarkable elevation in SWT in nearby channels, likely attributed to thermal bath activities in the town. In contrast, the lowest thermal impact was observed in smaller towns. For example, in Tiszafüred, which is famous for eco-tourism and water sports activities, and in Vásárosnamény where agriculture is predominant.

4.4.2. Influence of Shading and Groundwater Inflow

A sudden decline in SWT was noticed at certain channel sections (Figures 5 and 6H–I), where refugia were created to maintain biodiversity and ecosystem resilience. Since these channel sections are relatively far from confluences, they are likely to experience SWT declines due to factors such as shade and vegetation along riverbanks [51], groundwater inflow [52], thermal stratification, local anthropogenic activities, or a combination thereof. However, further field investigation and collection of in situ data, particularly regarding groundwater inflow, are necessary to determine the precise drivers of SWT decline. Given the seasonal variations in vegetation cover, surface and groundwater hydrology, and environmental factors, the magnitude of SWT decline varied across the months, with higher declines typically observed in summer and spring. This variability may also explain the sudden SWT declines observed in a channel section adjacent to Tisza Lake (Figure 6G), specifically in June. The upstream part of Tisza Lake, adjacent to the cooled river channel section, exhibits lower temperatures than the downstream part, suggesting

that the sudden decline in the river channel is primarily due to significant seepage from the lake into the river during the given period. Interestingly, the reduced SWT in the upstream part of the lake may be attributed to greater depth, the presence of shading, thermal stratification, and fewer anthropogenic activities. Nonetheless, comprehensive monitoring efforts focusing on the lake's hydrodynamics, geomorphology, and thermal stratification are warranted to fully understand these dynamics.

4.4.3. Influence of Dams

The three dams along the Tisza River (i.e., the Tiszalök, Kisköre, and Novi Bečej dams) showed a thermal pollution pattern similar to many dams reported in the literature, e.g., the Keepit Dam in Naomi River, Australia [53], Paso de las Piedras Dam in Sauce Grande River, Argentina [54], and Danjiangkou Dam in Han River, China [2]. Specifically, upstream of these dams, there is a rise in SWT due to reduced flow velocity, decreased turbulence, and increased water surface area in the reservoir, allowing for greater absorption of solar radiation and elevated warming. Meanwhile, downstream of the dams, SWT tends to decline due to thermal stratification in the reservoir upstream and the release of cooler water from the hypolimnion layer. However, the size of the dam, inflow and outflow rates, operational schemas, and the location of withdrawal points significantly influence the thermal pattern and its magnitude [54]. Notably, these variations contribute to slight differences in the thermal patterns observed among the three dams on the Tisza. For instance, water is occasionally released from the surface (epilimnion) at the Tiszalök Dam, while at the Kisköre and Novi Bečej dams, it is consistently released from the bottom (hypolimnetic). This distinction is crucial because epilimnetic withdrawal promotes stronger thermal stratification and stability, whereas hypolimnetic withdrawal weakens thermal stratification and stability [55].

4.4.4. Influence of Tributaries

Tributaries play an important role in shaping the longitudinal thermal profile of the Tisza, though their influence showed notable variability across the months, with localized effects and potential thermal stratification. Most probably (75%), the tributaries tend to warm the water of the Tisza throughout the year. Specifically, during summer and spring, tributaries often have warmer water due to reduced volume and increased absorption of solar radiation, thereby warming the water of the Tisza. Meanwhile, in winter and autumn, when tributaries are fed by snowmelt or cooler upstream sources, they can cool the water of the Tisza. However, this stereotype can vary, because of the complex interplay of factors affecting the thermal conditions of tributaries (e.g., catchment landscape, anthropogenic activities, environmental conditions, vegetation cover, regional climate, and elevation of the catchment) as well as their interactions with the main river. For instance, water from the Maros River decreased the SWT in the Tisza by 0.3 °C in July, likely due to cooler water originating from the Transylvanian mountains during summer rainfall and the greater flow velocity of the tributary. Interestingly, the findings revealed a weak correlation between the mean discharge of the tributaries and the SWT difference upstream and downstream of their confluence with the Tisza. This was evidenced by a significant difference of 3.36 °C in the low-discharge Zagyva River (9 m^3/s) and a slight difference of 0.012 °C in the high-discharge Maros River (150 m^3/s). This discrepancy can be attributed to seasonal variability in the tributaries' temperature and discharge, thermal and mixing patterns, and impoundment effects, highlighting the complexity of the thermal effects of tributaries into the main river.

4.5. Long-Term Evaluation of the Surface Water Temperature of the Tisza and Global Warming

The analysis of the SWT of the Tisza River at the Mindszent site between 1984 and 2024 revealed a significant upward trend at an annual rate of 0.068 °C, totaling 2.74 °C over the 40-year study period. This finding aligns with global warming trends observed

in rivers worldwide due to climate change, although the warming rate observed in the Tisza River is higher than the global average of 0.046 °C/year [56]. A higher increasing rate of 0.05–0.15 °C/year was reported in the Rhine River, based on 35-year (1980–2015) analysis [57], while comparable rates were reported in the Warta River, Poland (0.043–0.061 °C/year; 1984–2020) [56] and a lower rate was reported in the Vistula River, Poland (0.029–0.046 °C/year; 1984–2020) [8]. Interestingly, the observed warming rate in the Tisza River is similar to that in the Bracciano and Martignano lakes in Italy (0.053 °C/year) between 1984 and 2019, using Landsat images [58]. Although rivers and lakes have dissimilar thermal regimes, the long-term nature of the study period, pervasive global warming impacts, proximity of geographical locations, and similarity in long-term environmental and hydrological factors could lead to similar warming rates in both water bodies. Additionally, the warming rate in the Tisza between 2000 and 2019 (0.133 °C/year) was 2.3 times higher than the warming rate observed during the entire study period (1984–2019), which is consistent with what was reported in the Italian lakes.

This warming trend is primarily attributed to rising air temperatures, variations in precipitation patterns, and extreme meteorological events. These changes not only have negative consequences for ecological health, water quality, and hydrological processes in riverine systems but also for the economic utilization of water (e.g., for fishing and cooling water in industry). Specifically, the thermal regime change of a river can alter species distributions, reduce dissolved oxygen levels, increase the risk of harmful algal blooms, and intensify extreme hydrological events. Therefore, implementing comprehensive monitoring programs and adaptive management plans is crucial to mitigate the negative impacts of climate change not only in the Tisza River but also in rivers globally.

4.6. Limitations of Landsat-Based SWT Estimates

Although the Landsat satellites provide valuable data for evaluating the thermal dynamics of the Tisza River in response to natural and human factors, they still have some limitations that hinder accurate and efficient assessment. For instance, the coarse spatial resolution of thermal bands (60–120 m) leads to inaccurate SWT estimation, especially in narrow channels and at riverbanks, due to the occurrence of mixed pixels and the presence of shallow water. Additionally, this resolution hinders the accurate detection and monitoring of thermal plumes resulting from effluents of nuclear power plants, WWTPs, and industrial activities, particularly when the temperature difference between the effluent and the river is low. Seasonal changes in the hydro-morphological characteristics of a river, which influence river size and depth, can affect thermal data acquisition by satellites. The low temporal resolution of Landsat satellites—16 days—can result in the loss of important SWT data, especially in highly dynamic rivers with rapid temperature changes. Cloud cover also leads to discontinuous thermal profile data, particularly when assessing the entire catchment of a river. Furthermore, thermal data are highly influenced by atmospheric conditions and the applied correction model. Typically, Landsat satellites provide thermal data only for the very surface layer of water, so the thermal regime of the entire depth of the river is not captured.

5. Conclusions

The lack of adequate water temperature monitoring systems in rivers poses a challenge to comprehensively assessing thermal dynamics over space and time. In the meantime, the synoptic coverage and relatively frequent imaging of the TIR remote sensing techniques could offer a practical alternative. In this study, Landsat satellites and in situ water temperature data were used to (1) evaluate the accuracy of Landsat-based SWT estimation across different channel sections with varying sizes; (2) conduct a thorough analysis of SWT dynamics in the medium-sized Tisza River in Central Europe, examining its response to natural and anthropogenic factors throughout the year; and (3) assess the influence of global warming on SWT trends in the river by analyzing 438 historical Landsat images spanning from 1984 to 2024.

The study recommends using Landsat TIR data for estimating SWT in channel sections covering ≥ 3 pixels, achieving high accuracy ($R^2 = 0.99$; RMSE = 1.43 °C). Meanwhile, estimation accuracy gradually declined below this threshold (i.e., 1.5 pixels: $R^2 = 0.94$; RMSE = 3.99 °C; 0.7 pixels: $R^2 = 0.92$; RMSE = 4.73 °C), with a tendency to overestimate temperatures. Challenges such as cloud cover and a relatively long revisit time (16 days) limit the continuous provision of thermal data at large scales.

The variability in solar radiation, hydrological conditions, and day–night cycles throughout the year led to changes in the thermal diurnal cycle across different months. The longitudinal thermal profile of the Tisza River revealed a generally uniform pattern, though slight increases, decreases, and complex trends were observed across months, highlighting the diverse factors influencing its thermal profile and seasonal variations. Specifically, urban areas associated with urban heat islands (e.g., Szolnok and Szeged), showed elevated SWT in nearby channels due to industrial and transportation activities. Conversely, urban areas characterized by tourism and agriculture exerted a lesser influence on SWT. Groundwater inflow and riparian shading created thermal refugia (SWT declines) for organisms, although the magnitude of these declines varied seasonally. Dams along the Tisza River increased the SWT upstream in their reservoirs and decreased it downstream, with varying magnitudes influenced by dam characteristics and operational schemes. Tributaries generally warmed the Tisza's water, particularly in summer and spring, yet this role could vary due to changes in catchment characteristics and hydrometeorological conditions throughout the year. The water temperature of the Tisza is influenced by global warming, evidenced by an annual SWT increase rate of 0.068 °C between 1984 and 2024.

The Landsat satellites provided valuable thermal data for the medium-sized Tisza River for evaluating the spatiotemporal thermal dynamics of the river in response to various natural and anthropogenic factors. However, the relatively coarse spatial resolution of thermal bands (60–120 m), the low temporal resolution of 16 days, and the occurrence of cloud cover limit its potential for effectively evaluating narrow sections and the large scale of the entire river. Notably, these data are crucial for understanding the thermal profiles of rivers and their implications for river ecology. Additionally, they are beneficial for developing adaptive measures to address climate change impacts and for implementing restoration plans.

Author Contributions: Conceptualization, F.K., T.K., and S.B.; methodology, F.K., and A.M.; software, A.M. and A.B; formal analysis, A.M., T.K., and F.K.; resources, T.K.; draft preparation, A.M. and T.K; review and editing, T.K., F.K., A.M., S.B., and A.B; supervision, T.K., F.K., and S.B; funding acquisition, F.K. All authors have read and agreed to the published version of the manuscript.

Funding: Project no. TKP2021-NVA-09 was implemented with support provided by the Ministry of Innovation and Technology of Hungary from the National Research, Development and Innovation Fund, financed under the TKP2021-NVA funding scheme. A.M. is funded by a scholarship (grant number: SHE-13402-004/2020) under the joint executive program between the Arab Republic of Egypt and Hungary.

Data Availability Statement: The applied data in this study are freely available at https://www.danubehis.org/ (accessed on 25 February 2024) and https://dataspace.copernicus.eu (accessed on 20 February 2024).

Conflicts of Interest: The authors declare no conflicts of interest.

Appendix A

Table A1. Characteristics of the mosaicked four Landsat 8 and 9 images each month, covering the entire Tisza River.

Month	Path	Row	Date	Month	Path	Row	Date
January	187	28	8 January 2023	July	187	28	11 July 2023
	187	27	24 January 2023		187	27	3 July 2023
	186	27	1 January 2023		186	27	20 July 2023
	185	27	2 January 2023		185	27	29 July 2023
February	187	28	9 February 2023	August	187	28	20 August 2023
	187	27	9 February 2023		187	27	20 August 2023
	186	27	10 February 2023		186	27	21 August 2023
	185	27	20 February 2023		185	27	22 August 2023
March	187	28	13 March 2023	September	187	28	5 September 2023
	187	27	13 March 2023		187	27	5 September 2023
	186	27	22 March 2023		186	27	6 September 2023
	185	27	24 March 2023		185	27	7 September 2023
April	187	28	30 April 2023	October	187	28	23 October 2023
	187	27	30 April 2023		187	27	23 October 2023
	186	27	23 April 2023		186	27	16 October 2023
	185	27	24 April 2023		185	27	17 October 2023
May	187	28	8 May 2023	November	187	28	16 November 2023
	187	27	8 May 2023		187	27	16 November 2023
	186	27	9 May 2023		186	27	11 September 2023
	185	27	10 May 2023		185	27	26 November 2023
June	187	28	1 June 2023	December	187	28	18 December 2023
	187	27	1 June 2023		187	27	18 December 2023
	186	27	2 June 2023		186	27	27 December 2023
	185	27	3 June 2023		185	27	20 December 2023

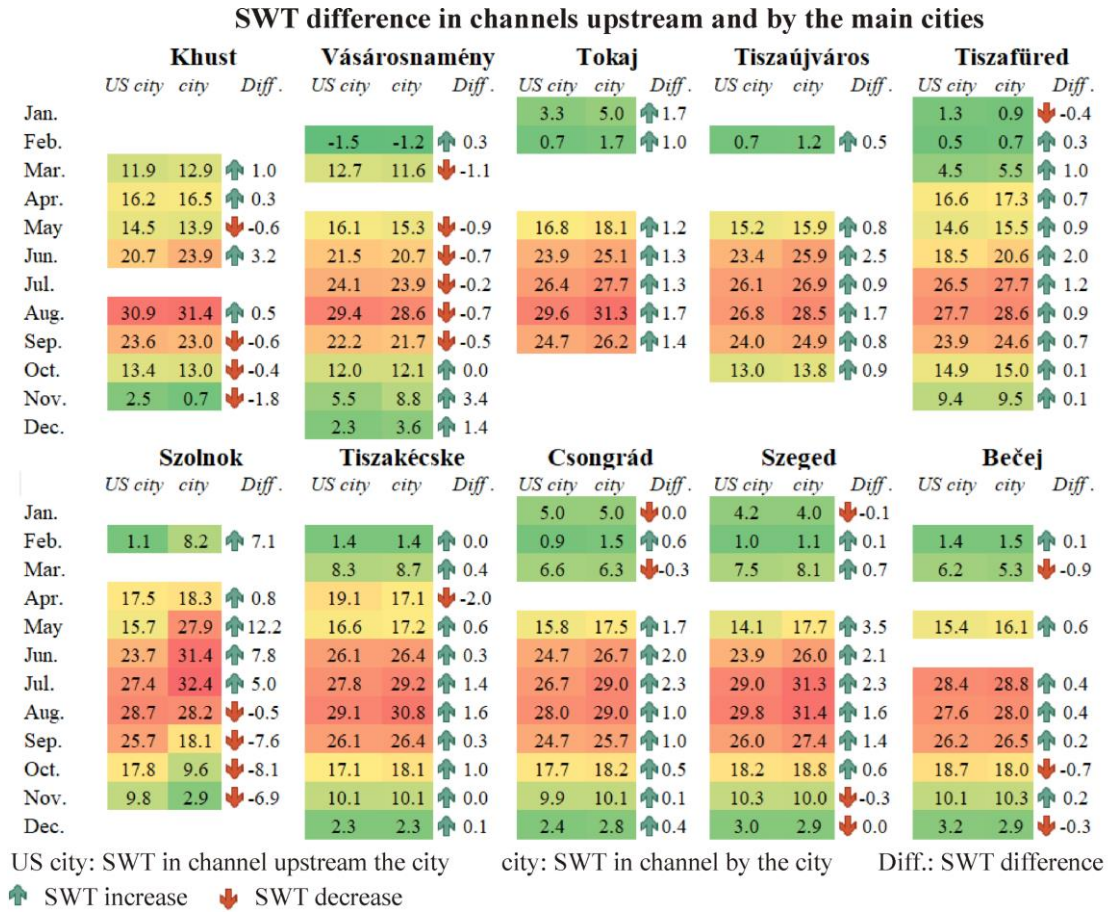

Figure A1. Surface water temperature (SWT) differences between channels located upstream of ten major cities along the Tisza River and those located adjacent to the cities.

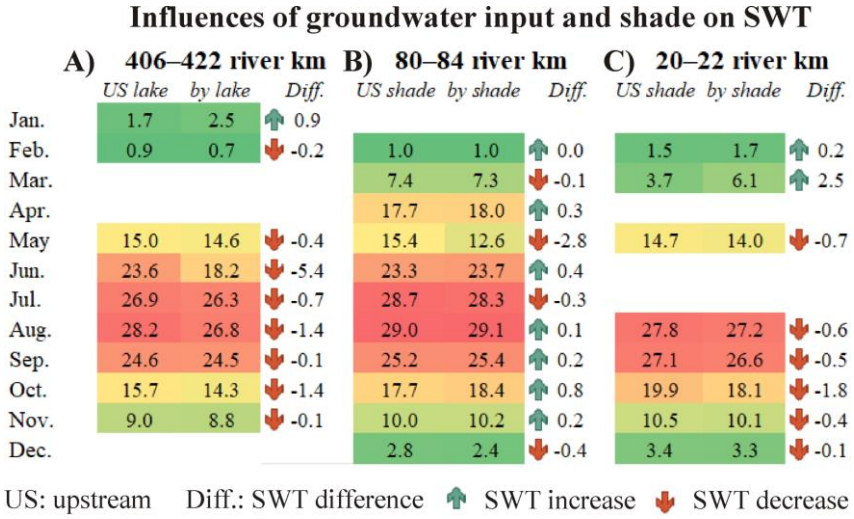

Figure A2. Surface water temperature (SWT) differences between channels upstream of Tisza Lake and adjacent to the lake (**A**) and between upstream and adjacent shaded channel sections (**B**,**C**).

References

1. Webb, B.W.; Hannah, D.M.; Moore, R.D.; Brown, L.E.; Nobilis, F. Recent advances in stream and river temperature research. *Hydrol. Process.* **2008**, *22*, 902–918. https://doi.org/10.1002/hyp.6994.
2. Zhao, J.; Li, H.; Cai, X.; Chen, F.; Wang, L.; Yu, D.; Li, C.A. Long-term (2002–2017) impacts of Danjiangkou dam on thermal regimes of downstream Han River (China) using Landsat thermal infrared imagery. *J. Hydrol.* **2020**, *589*, 125135. https://doi.org/10.1016/j.jhydrol.2020.125135.

3. Ling, F.; Foody, G.M.; Du, H.; Ban, X.; Li, X.; Zhang, Y.; Du, Y. Monitoring Thermal Pollution in Rivers Downstream of Dams with Landsat ETM+ Thermal Infrared Images. *Remote Sens.* **2017**, *9*, 1175. https://doi.org/10.3390/rs9111175.
4. Yao, Y.; Huang, X.; Liu, J.; Zheng, C.; He, X.; Liu, C. Spatiotemporal variation of river temperature as a predictor of groundwater/surface-water interactions in an arid watershed in China. *Hydrogeol. J.* **2015**, *23*, 999–1007. https://doi.org/10.1007/s10040-015-1265-y.
5. Toffolon, M.; Piccolroaz, S. A hybrid model for river water temperature as a function of air temperature and discharge. *Environ. Res. Lett.* **2015**, *10*, 114011. https://doi.org/10.1088/1748-9326/10/11/114011.
6. Mejia, F.H.; Torgersen, C.E.; Berntsen, E.K.; Maroney, J.R.; Connor, J.M.; Fullerton, A.H.; Ebersole, J.L.; Lorang, M.S. Longitudinal, lateral, vertical and temporal thermal heterogeneity in a large impounded river: Implications for cold-water refuges. *Remote Sens.* **2020**, *12*, 1–1386. https://doi.org/10.3390/rs12091386.
7. Fullerton, A.H.; Torgersen, C.E.; Lawler, J.J.; Faux, R.N.; Steel, E.A.; Beechie, T.J.; Ebersole, J.L.; Leibowitz, S.G. Rethinking the longitudinal stream temperature paradigm: Region-wide comparison of thermal infrared imagery reveals unexpected complexity of river temperatures. *Hydrol. Process.* **2015**, *29*, 4719–4737. https://doi.org/10.1002/hyp.10506.
8. Rajesh, M.; Rehana, S. Impact of climate change on river water temperature and dissolved oxygen: Indian riverine thermal regimes. *Sci. Rep.* **2022**, *12*, 9222. https://doi.org/10.1038/s41598-022-12996-7.
9. Takács, K.; Kern, Z.; Pásztor, L. Long-term ice phenology records from eastern–central Europe. *Earth Syst. Sci. Data* **2018**, *10*, 391–404.
10. Tassone, S.J.; Besterman, A.F.; Buelo, C.D.; Ha, D.T.; Walter, J.A.; Pace, M.L. Increasing heatwave frequency in streams and rivers of the United States. *Limnol. Oceanogr. Lett.* **2023**, *8*, 295–304. https://doi.org/10.1002/lol2.10284.
11. Georges, B.; Michez, A.; Piegay, H.; Huylenbroeck, L.; Lejeune, P.; Brostaux, Y. Which environmental factors control extreme thermal events in rivers? A multi-scale approach (Wallonia, Belgium). *PeerJ* **2021**, *9*, e12494. https://doi.org/10.7717/peerj.12494.
12. Qicai, L. Influence of dams on river ecosystem and its countermeasures. *J. Water Resour. Prot.* **2011**, *3*, 60–66. https://doi.org/10.4236/jwarp.2011.31007.
13. Seyedhashemi, H.; Moatar, F.; Vidal, J.-P.; Diamond, J.S.; Beaufort, A.; Chandesris, A.; Valette, L. Thermal signatures identify the influence of dams and ponds on stream temperature at the regional scale. *Sci. Total Environ.* **2021**, *766*, 142667. https://doi.org/10.1016/j.scitotenv.2020.142667.
14. Csoma, J.; Szilágyi, J.; Zboray, K. Water, sediment and ice conditions of the reservoir of Tiszalök, Hungary (A tiszalöki duzzasztott tér víz-, hordalék- és jéglevonulási viszonyai.). *Vízügyi Közlemények* **1967**, *49/2*, 249–259.
15. Schwanen, C.A.; Schwarzbauer, J. Structural Diversity of Organic Contaminants in a meso-scaled River System. *Water Air Soil Pollut.* **2022**, *233*, 33. https://doi.org/10.1007/s11270-022-05503-1.
16. Aristi, I.; von Schiller, D.; Arroita, M.; Barceló, D.; Ponsatí, L.; García-Galán, M.J.; Sabater, S.; Elosegi, A.; Acuña, V. Mixed effects of effluents from a wastewater treatment plant on river ecosystem metabolism: Subsidy or stress? *Freshw. Biol.* **2015**, *60*, 1398–1410. https://doi.org/10.1111/fwb.12576.
17. Li, X.; Jiang, G.; Tang, X.; Zuo, Y.; Hu, S.; Zhang, C.; Wang, Y.; Wang, Y.; Zheng, L. Detecting Geothermal Anomalies Using Multi-Temporal Thermal Infrared Remote Sensing Data in the Damxung–Yangbajain Basin, Qinghai–Tibet Plateau. *Remote Sens.* **2023**, *15*, 4473. https://doi.org/10.3390/rs15184473.
18. Handcock, R.N.; Torgersen, C.E.; Cherkauer, K.A.; Gillespie, A.R.; Tockner, K.; Faux, R.N.; Tan, J. Thermal Infrared Remote Sensing of Water Temperature in Riverine Landscapes. In *Fluvial Remote Sensing for Science and Management*; John Wiley & Sons, Ltd.: Hoboken, NJ, USA, 2012; pp. 85–113.
19. Fricke, K.; Baschek, B. Temperature monitoring along the Rhine River based on airborne thermal infrared remote sensing: Estimation of in situ water temperatures and inflow detection compared to artificial satellite data. *J. Appl. Remote Sens.* **2015**, *9*, 095067.
20. Torgersen, C.E.; Faux, R.N.; Mcintosh, B.A.; Poage, N.J.; Norton, D.J. Airborne thermal remote sensing for water temperature assessment in rivers and streams. *Remote Sens. Environ.* **2001**, *76*, 386–398.
21. Reinart, A.; Reinhold, M. Mapping surface temperature in large lakes with MODIS data. *Remote Sens. Environ.* **2008**, *112*, 603–611. https://doi.org/10.1016/j.rse.2007.05.015.
22. Lászlóffy, W. Tisza River: Construction and Water Management in the Tisza Water Regime. 1982. Available online: https://journals.sagepub.com/doi/10.1177/030913338400800311 (accessed on 26 August 2024).
23. Balint, Z.; Tóth, S. Flood protection in the Tisza Basin. In *Proceedings of the Flood Risk Management: Hazards, Vulnerability and Mitigation Measures*; Springer: Dordrecht, The Netherlands, 2006; pp. 185–197.
24. Mohsen, A.; Balla, A.; Kiss, T. High Spatiotemporal Resolution Analysis on Suspended Sediment and Microplastic Transport of a Lowland River. *Sci. Total Environ.* **2023**, *902*, 166188. https://doi.org/10.1016/j.scitotenv.2023.166188.
25. Leščešen, I.; Dolinaj, D.; Pantelić, M.; Telbisz, T.; Varga, G. Hydrological drought assessment of the Tisza river. *J. Geogr. Inst. Jovan Cvijic SASA* **2020**, *70*, 89–100.
26. Kiss, T.; Gönczy, S.; Nagy, T.; Mesaroš, M.; Balla, A. Deposition and Mobilization of Microplastics in a Low-Energy Fluvial Environment from a Geomorphological Perspective. *Appl. Sci.* **2022**, *12*, 4367. https://doi.org/10.3390/app12094367.
27. Sipos, G.; Blanka, V.; Mezősi, G.; Kiss, T.; van Leeuwen, B. Effect of Climate Change on the Hydrological Character of River Maros, Hungary-Romania. *J. Environ. Geogr.* **2014**, *7*, 49–56. https://doi.org/10.2478/jengeo-2014-0006.

28. János, T.; Bernadett, G.; Bódi, E.B.; Magyar, T.; Nagy, A. Evaluation of water demand supply on Tisza River Basin. In Proceedings of the 3rd World Irrigation Forum (WIF3), Bali, Indonesia, 1–7 September 2019.
29. Mohsen, A.; Kovács, F.; Kiss, T. Remote Sensing of Sediment Discharge in Rivers using Sentinel-2 Images and Machine-learning Algorithms. *Hydrology* **2022**, *9*, 88. https://doi.org/10.3390/hydrology9050088.
30. ICPDR. *Analysis of the Tisza River Basin 2007*; International Commission for the Protection of the Danube River, Vienna International Centre/D0412: Vienna, Austria, 2007; p. 136.
31. FehérJános. *Updated Integrated Tisza River Basin Management Plan*; Interreg Europe: Lille, France, 2019.
32. Lovász, G. Water temperatures of the Danube and Tisza Rivers in Hungary. *Hung. Geogr. Bull.* **2012**, *61*, 317–325.
33. Fehér, Z.Z.; Rakonczai, J. Analysing the sensitivity of Hungarian landscapes based on climate change induced shallow groundwater fluctuation. *Hung. Geogr. Bull.* **2019**, *68*, 355–372.
34. Eliáš jun, P.; Dítě, D.; Dítě, Z. Halophytic Vegetation in the Pannonian Basin: Origin, Syntaxonomy, Threat, and Conservation. In *Handbook of Halophytes: From Molecules to Ecosystems towards Biosaline Agriculture*; Grigore, M.-N., Ed.; Springer International Publishing: Cham, Switzerland, 2021; pp. 287–324.
35. Trásy-Havril, T.; Szkolnikovics-Simon, S.; Mádl-Szőnyi, J. How Complex Groundwater Flow Systems Respond to Climate Change Induced Recharge Reduction? *Water* **2022**, *14*, 3026. https://doi.org/10.3390/w14193026.
36. Ptak, M.; Choiński, A.; Piekarczyk, J.; Pryłowski, T. Applying Landsat Satellite Thermal Images in the Analysis of Polish Lake Temperatures. *Pol. J. Environ. Stud.* **2017**, *26*, 2159–2165. https://doi.org/10.15244/pjoes/69444.
37. Lamaro, A.A.; Mariñelarena, A.; Torrusio, S.E.; Sala, S.E. Water surface temperature estimation from Landsat 7 ETM+ thermal infrared data using the generalized single-channel method: Case study of Embalse del Río Tercero (Córdoba, Argentina). *Adv. Space Res.* **2013**, *51*, 492–500. https://doi.org/10.1016/j.asr.2012.09.032.
38. Jiang, L.; Wu, H.; Kimball, J.; Tao, J. Streamflow temperature estimation based on Landsat thermal infrared and optical bands data. In Proceedings of the AGU Fall Meeting 2021, New Orleans, LA, USA, 13–17 December 2021; pp. H25F–1103.
39. Teixeira Pinto, C.; Jing, X.; Leigh, L. Evaluation analysis of Landsat level-1 and level-2 data products using in situ measurements. *Remote Sens.* **2020**, *12*, 2597.
40. Sayler, K.; Zanter, K. *Landsat 8 Collection 1 (C1) Land Surface Reflectance Code (LaSRC) Product Guide*; LSDS-1368 Version; Department Interior United States Geological Survey: Reston, VA, USA, 2020; Volume 3.
41. McFeeters, S.K. The use of the Normalized Difference Water Index (NDWI) in the Delineation of Open Water Features. *Int. J. Remote Sens.* **1996**, *17*, 1425–1432. https://doi.org/10.1080/01431169608948714.
42. Otsu, N. A threshold Selection Method from Gray-level Histograms. *IEEE Trans. Syst. Man Cybern.* **1979**, *9*, 62–66. https://doi.org/10.1109/TSMC.1979.4310076.
43. ESA. Available online: https://step.esa.int/main/download/snap-download/ (accessed on 20 June 2021).
44. Mann, H.B. Nonparametric Tests Against Trend. *Econom. J. Econom. Soc.* **1945**, *13*, 245–259. https://doi.org/10.2307/1907187.
45. Kendall, M. Rank Correlation Measures. *Charles Griffin Lond.* **1975**, *202*, 15.
46. IBM. Statistical Package for Social Sciences (SPSS) Software. Available online: https://www.ibm.com/analytics/us/en/technology/spss/ (accessed on 25 May 2022).
47. Ali, S.A.; Parvin, F.; Ahmad, A. Retrieval of Land Surface Temperature from Landsat 8 OLI and TIRS: A Comparative Analysis Between Radiative Transfer Equation-Based Method and Split-Window Algorithm. *Remote Sens. Earth Syst. Sci.* **2023**, *6*, 1–21. https://doi.org/10.1007/s41976-022-00079-0.
48. Niedrist, G.H. Substantial warming of Central European mountain rivers under climate change. *Reg. Environ. Chang.* **2023**, *23*, 43. https://doi.org/10.1007/s10113-023-02037-y.
49. Stanford, J.A.; Ward, J.V. Revisiting the serial discontinuity concept. *Regul. Rivers: Res. Manag. Int. J. Devoted River Res. Manag.* **2001**, *17*, 303–310.
50. CityPopulation. Available online: https://www.citypopulation.de/en/ (accessed on 12 June 2024).
51. Brosofske, K.D.; Chen, J.; Naiman, R.J.; Franklin, J.F. Harvesting effects on microclimatic gradients from small streams to uplands in western Washington. *Ecol. Appl.* **1997**, *7*, 1188–1200. https://doi.org/10.1890/1051-0761(1997)007[1188:HEOMGF]2.0.CO;2.
52. Keery, J.; Binley, A.; Crook, N.; Smith, J.W.N. Temporal and spatial variability of groundwater–surface water fluxes: Development and application of an analytical method using temperature time series. *J. Hydrol.* **2007**, *336*, 1–16. https://doi.org/10.1016/j.jhydrol.2006.12.003.
53. Preece, R.M.; Jones, H.A. The effect of Keepit Dam on the temperature regime of the Namoi River, Australia. *River Res. Appl.* **2002**, *18*, 397–414. https://doi.org/10.1002/rra.686.
54. Casado, A.; Hannah, D.M.; Peiry, J.-L.; Campo, A.M. Influence of dam-induced hydrological regulation on summer water temperature: Sauce Grande River, Argentina. *Ecohydrology* **2013**, *6*, 523–535. https://doi.org/10.1002/eco.1375.
55. Kerimoglu, O.; Rinke, K. Stratification dynamics in a shallow reservoir under different hydro-meteorological scenarios and operational strategies. *Water Resour. Res.* **2013**, *49*, 7518–7527. https://doi.org/10.1002/2013WR013520.
56. Gizińska, J.; Sojka, M. How Climate Change Affects River and Lake Water Temperature in Central-West Poland—A Case Study of the Warta River Catchment. *Atmosphere* **2023**, *14*, 330. https://doi.org/10.3390/atmos14020330.

57. Itsukushima, R.; Ohtsuki, K.; Sato, T. Drivers of rising monthly water temperature in river estuaries. *Limnol. Oceanogr.* **2024**, *69*, 589–603. https://doi.org/10.1002/lno.12507.
58. De Santis, D.; Del Frate, F.; Schiavon, G. Analysis of Climate Change Effects on Surface Temperature in Central-Italy Lakes Using Satellite Data Time-Series. *Remote Sens.* **2022**, *14*, 117. https://doi.org/10.3390/rs14010117.